

Differential Path Considerations

T. A. TEN BRUMMELAAR
CHARA, GEORGIA STATE UNIVERSITY, ATLANTA, GA 30303

N.1. INTRODUCTION

This Appendix describes a formulation of the differential air path problem for the CHARA Array. This problem arises because we plan to use an OPLE in air rather than vacuum as most other groups have done. Since air is a dispersive medium, each wavelength will have a different optical path length. This can be corrected to a large extent by placing an extra piece of glass in each arm of the interferometer. The problem then becomes analogous to doublet achromat design where, in this case, the air path takes the place of one piece of glass. Atmospheric refraction and field of view considerations also amount to changing the differential paths within the interferometer. All three effects can therefore be considered to be aspects of the same problem.

It is assumed that we will use many, programmable, narrow-band channels evenly distributed in wavenumber space to get the equivalent of a larger bandpass as suggested by J. Beletic. This differs from the treatment of dispersion by Tango (1990) in that he looks at the problem of a single, large-bandwidth, pixel. The calculations below are largely based on an internal report by Traub (1990) for the IOTA project. The technical report on dispersion effects in BOA by Ling (1990) was also consulted, although the solution proposed for BOA (rotating glass plates) would not be suitable for CHARA as our air paths are much larger.

The basic results are that while no correction is required in the IR band, in the 0.6 to 0.8 micron band dispersion must be corrected by using approximately 0.45 mm of BK7 glass for every meter of differential air path. Thus for a 350 m baseline at a zenith angle of 50° a total thickness of some 12 cm will be required. Other glasses may have better characteristics but are yet to be investigated. A second effect of adding glass to one arm is to move the fringes up to tens of centimeters away from the original white light position. This will make simultaneous observations in the visible and IR bands difficult if not impossible. However, if one is willing to forgo science measurements in the visible system and use that system only for fringe tracking without dispersion correction, it should then be possible to simultaneously use the IR system for imaging data.

N.2. GEOMETRY

We consider a single pair of telescopes with the geometry as shown in Figure N.1. Two beams are shown in this diagram, one indicating the tracking center at a true zenith angle of θ and a second beam looking at an angle α away from this position. Both beams are then refracted by the atmosphere and reach the telescopes with an angular separation of β . This angle is magnified by the telescopes by a factor of M and sent through the interferometer optics. One arm passes through the OPLE whose length is x_{OPLE} , the rest of the internal paths are assumed to be identical. Both beams then pass through atmospheric refraction correctors (ARC) so that all beams are, to first order, parallel. Finally, one arm passes through a longitudinal dispersion corrector (LDC) before the beams are combined to form fringes. In the calculations to follow we define two fixed wavelengths: the tracking

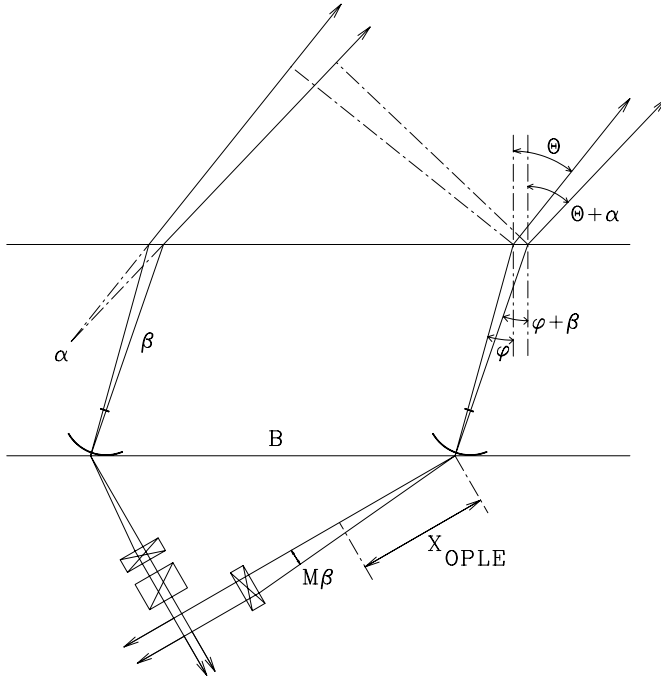


FIGURE N.1. Definition of geometry used to calculate differential path effects.

wavelength λ_{track} is the wavelength used for the detector of the tip/tilt servo and defines the pointing position; the phasing wavelength λ_{ph} defines the wavelength used to track the fringes, normally referred to as the phase center.

N.3. ATMOSPHERIC REFRACTION

The effect of atmospheric refraction is well understood and easily corrected using Risley prisms. The change in zenith angle introduced by the atmosphere is

$$\Delta\theta = \left(\frac{1}{n_{\text{air}}(\lambda)} - 1 \right) \tan\theta. \quad (\text{N.1})$$

Note that this expression is different to that normally cited since we have defined θ to be the true rather than the observed zenith angle. A plot of this angular change for a zenith angle of 50° and a range of wavelengths is given in Figure N.2. Thus, if the angular separation of the beam from the tracking center is α above the atmosphere, it will be

$$\beta(\lambda) = \frac{1}{n_{\text{air}}(\lambda)} (\tan\theta + \alpha) - \frac{1}{n_{\text{air}}(\lambda_{\text{track}})} \tan\theta \quad (\text{N.2})$$

DIFFERENTIAL PATH CONSIDERATIONS

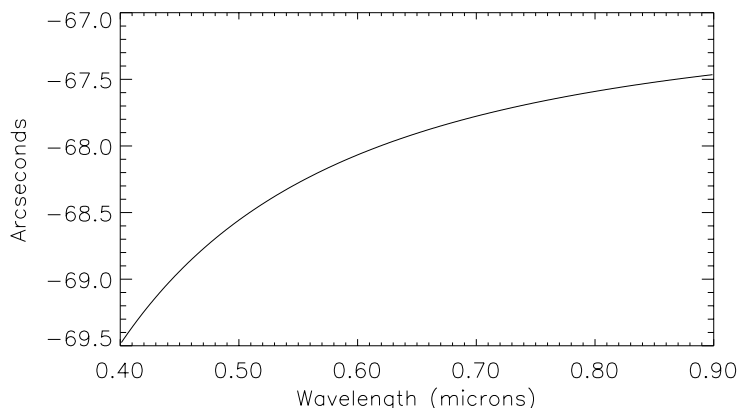


FIGURE N.2. The change in the zenith angle due to atmospheric refraction at an average zenith angle of 50° .

after being refracted by the atmosphere. Since the refractive index of air changes slowly with wavelength this expression can be approximated by

$$\beta(\lambda) = \frac{\alpha}{n_{\text{air}}(\lambda)}. \quad (\text{N.3})$$

This difference in angle between the tracking center and the direction of observation will have two effects, both due entirely to the path through the OPLE as all other lengths of the interfering beams are identical. The first effect will be a differential optical path of $x_{\text{OPLE}}/\cos(M\beta(\lambda))$, a second order effect that can be ignored in this analysis. For example, if $x_{\text{OPLE}} = 280$ m, $\alpha = 1''\lambda_{\text{track}} = 0.4 \mu\text{m}$ and $\lambda = 0.55 \mu\text{m}$, the difference in path length is $0.8 \mu\text{m}$. As the analysis that follows will show, this is much less than the size of the fringe envelope. The second effect is a beam displacement. With the numbers used above, this amounts to a beam displacement of 2 cm which, after passing through the beam reducing telescopes, becomes 4 mm. The ARC will then ensure that, although displaced, the beams are parallel to the optical axis. Thus, since we are using lenses to form images in all of the detectors and as long as the size of the optics is chosen so that no aliasing will occur, this beam displacement will have little or no affect on fringe formation. We therefore conclude that atmospheric refraction is not a first-order problem for the CHARA array, and the ARC can be placed at the back end of the interferometer, as long as it is as close as possible to the beam reducing telescopes. Of course, if we decide to go for larger apertures, and therefore larger beam reduction at the telescopes, these effects increase proportionately. It may then become necessary to place the ARCs out near the telescopes.

We conclude then that atmospheric refraction can be largely ignored and that Equation N.3 is a valid approximation. In order to test this, the analysis below was repeated with the full expression shown in Equation N.2 and including OPLE path differences. The results did not differ significantly from those presented below.

N.4. LONGITUDINAL DISPERSION

The differential air path of the two beams in the interferometer due to the OPLE results in different path lengths at different wavelengths. We hope to correct for this by placing a piece of glass in the beam that has the shortest air path. Therefore, to first order, we write the optical path length difference at a given wavelength between the two interfering beams as

$$\text{OPD} = \underbrace{B \sin(\theta + \alpha)}_{\text{Baseline Projection}} + \underbrace{n_{\text{glass}}(\lambda)d}_{\text{LDC}} - \underbrace{n_{\text{air}}(\lambda)x_{\text{OPLE}}}_{\text{OPLE}}. \quad (\text{N.4})$$

Here d is the thickness of the glass in the LDC. The length of the OPLE can then be defined as a displacement l from the position x_0 ,

$$x_{\text{OPLE}} = x_0 + l \quad (\text{N.5})$$

where x_0 is the OPLE position for white light fringes when $d = l = \alpha = 0$ and at some wavelength defining the phase center λ_{ph} . Thus

$$x_0 = \frac{1}{n_{\text{air}}(\lambda_{\text{ph}})} B \sin \theta. \quad (\text{N.6})$$

Since we know that the field of view α will be small, we can expand the sin term in Equation N.4 and write the optical path length difference as

$$\text{OPD} = B \sin \theta \left(1 - \frac{n_{\text{air}}(\lambda)}{n_{\text{air}}(\lambda_{\text{ph}})} \right) + n_{\text{glass}}(\lambda)d - n_{\text{air}}(\lambda)l + \alpha B \cos \theta. \quad (\text{N.7})$$

The detected fringe pattern at a single wavelength depends on this optical path length difference as follows

$$I(\nu) = 1 + V(\nu) \cos(2\pi\nu \text{OPD}), \quad (\text{N.8})$$

where we have now used the wavenumber $\nu = \frac{1}{\lambda}$ instead of the wavelength λ and $V(\nu)$ is the fringe visibility which is also a function of the wavenumber. This expression is integrated over some waveband centered on ν_0 and width $\Delta\nu$, assumed small, on each pixel of the detector, and therefore the detected fringe pattern in a single pixel will be

$$\begin{aligned} F(\nu_0, \Delta\nu) &= \frac{1}{\Delta\nu} \int_{\nu_0 - \frac{1}{\Delta\nu}}^{\nu_0 + \frac{1}{\Delta\nu}} I(\nu) d\nu \\ &= 1 + \frac{V(\nu_0)}{\Delta\nu} \int_{\nu_0 - \frac{1}{\Delta\nu}}^{\nu_0 + \frac{1}{\Delta\nu}} \cos 2\pi H(\nu) d\nu \end{aligned} \quad (\text{N.9})$$

where

$$H(\nu) = \nu \left[B \sin \theta \left(1 - \frac{n_{\text{air}}(\nu)}{n_{\text{air}}(\nu_{\text{ph}})} \right) + n_{\text{glass}}(\nu)d - n_{\text{air}}(\nu)l + \alpha B \cos \theta \right], \quad (\text{N.10})$$

and we have assumed that the visibility does not change substantially across the small bandpass $\Delta\nu$.

Because the bandpass is small, we can expand the refractive indices of air and glass around ν_0 so

$$n(\nu) = n(\nu_0) + n'(\nu_0)(\nu - \nu_0) + O(\Delta\nu^2) \quad (\text{N.11})$$

DIFFERENTIAL PATH CONSIDERATIONS

which results in

$$\begin{aligned}
 H(\nu) &= \nu B \sin \theta \left(1 - \frac{n_{\text{air}}(\nu_0)}{n_{\text{air}}(\nu_{\text{ph}})} - \frac{n'_{\text{air}}(\nu_0)}{n_{\text{air}}(\nu_{\text{ph}})}(\nu - \nu_0) \right) \\
 &\quad + d \left(n_{\text{glass}}(\nu_0) + n'_{\text{glass}}(\nu_0)(\nu - \nu_0) \right) \nu \\
 &\quad - l \left(n_{\text{air}}(\nu_0) + n'_{\text{air}}(\nu_0)(\nu - \nu_0) \right) \nu + \alpha B \nu \cos \theta.
 \end{aligned} \tag{N.12}$$

Next we use the new variable $\eta = \nu - \nu_0$ and, after a bit of algebra, find that

$$H(\nu) = \mathcal{A} + \mathcal{B}\eta + O(\eta^2) \tag{N.13}$$

where

$$\mathcal{A} = \nu_0 B \sin \theta \left(1 - \frac{n_{\text{air}}(\nu_0)}{n_{\text{air}}(\nu_{\text{ph}})} \right) + \nu_0 n_{\text{glass}}(\nu_0) d - \nu_0 n_{\text{air}}(\nu_0) l + \nu_0 \alpha B \cos \theta \tag{N.14}$$

and

$$\begin{aligned}
 \mathcal{B} &= -\nu_0 B \sin \theta \frac{n'_{\text{air}}(\nu_0)}{n_{\text{air}}(\nu_{\text{ph}})} + B \sin \theta \left(1 - \frac{n_{\text{air}}(\nu_0)}{n_{\text{air}}(\nu_{\text{ph}})} \right) \\
 &\quad + (\nu_0 n'_{\text{glass}}(\nu_0) + n_{\text{glass}}(\nu_0)) d - (\nu_0 n'_{\text{air}}(\nu_0) + n_{\text{air}}(\nu_0)) l + \alpha B \cos \theta.
 \end{aligned} \tag{N.15}$$

The detected signal in a single pixel as defined in Equation N.9 can then be calculated to yield

$$\begin{aligned}
 F(\nu_0, \Delta\nu) &= 1 + \frac{V(\nu_0)}{\Delta\nu} \int_{-\frac{\Delta\nu}{2}}^{\frac{\Delta\nu}{2}} \cos(2\pi [\mathcal{A} + \mathcal{B}\eta]) d\eta \\
 &= 1 + V(\nu_0) \frac{\text{sin} \mathcal{Z}}{\mathcal{Z}} \cos 2\pi \mathcal{A}
 \end{aligned} \tag{N.16}$$

where

$$\mathcal{Z} = \Delta\nu \pi \mathcal{B}. \tag{N.17}$$

The resulting fringe pattern consists of two parts: an oscillating cosine term, representing the fringes themselves, modulated by a sinc function, the Fourier transform of the square bandpass. Had we used some other form for the bandpass, this sinc function would become the Fourier transform of the filter function chosen. For example, if we were to use a Gaussian function for the bandpass the fringe envelope would also be a Gaussian. An example of some fringes is given in Figure N.3.

It is clear from Figure N.3 that the fringe pattern envelope peak will not be at the OPLE zero point $l = 0$ but at a position where $\mathcal{Z} = 0$. This will occur when $l = l_0$ where

$$l_0 = \frac{B \sin \theta \left[\left(1 - \frac{n_{\text{air}}(\nu_0)}{n_{\text{air}}(\nu_{\text{ph}})} \right) \Delta\nu - \nu_0 \frac{\Delta n_{\text{air}}}{n_{\text{air}}(\nu_{\text{ph}})} \right] + (\nu_0 \Delta n_{\text{glass}} + n_{\text{glass}}(\nu_0) \Delta\nu) d + \Delta\nu \alpha B \cos \theta}{\nu_0 \Delta n_{\text{air}} + n_{\text{air}}(\nu_0) \Delta\nu} \tag{N.18}$$

THE CHARA ARRAY

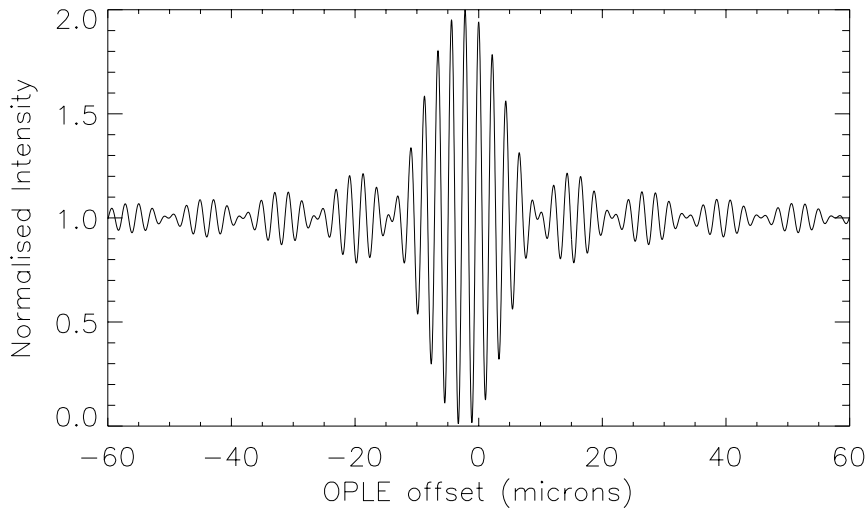


FIGURE N.3. The fringe pattern predicted for a bandpass of 2.0 to 2.4 microns, a phase center wavelength of 2.2 microns, a baseline of 8 meters and a zenith angle of 30° .

and we have made the further substitution

$$n'(\nu_0) \approx \frac{\Delta n}{\Delta \nu}. \quad (\text{N.19})$$

The fringe envelope will reach it's first minimum when $\mathcal{Z} = \pm\pi$. The width of the fringe envelope is therefore

$$\Delta l = \frac{2}{\nu_0 \Delta n_{\text{air}} + n_{\text{air}}(\nu_0) \Delta \nu}. \quad (\text{N.20})$$

Thus we see that the fringe envelope center moves away from the OPLE zero point and that this distance from the OPLE center depends on the baseline, the zenith angle, the field of view angle, the amount of glass used in the LDC, and the wavelength. Figure N.4 shows the position of the fringe envelope for a baseline of 350 meters, a zenith angle of 50° , no glass in the LDC, and for a range of 128 pixels spaced over the bandpass of 0.6 to 0.8 microns. This plot makes it clear why longitudinal dispersion correctors are required. Only a small range of pixels lie with the 5% loss range of the curve for any given OPLE position. Figure N.5 shows the same calculation except 11 cm of glass has been added in the LDC. Now that this extra glass has been inserted, the entire bandpass is contained within the 5% loss lines, indeed an even bigger bandpass could be corrected. Note, however, that the position of the fringes has been moved some 18 cm.

N.4.1. The Infrared Band

Using Equations N.18 and N.20, it is easy to generate similar plots for the infrared band. For example, Figure N.6 shows the fringe envelope for an IR band of 20 pixels covering 2 to 2.5 microns, once again with a baseline of 350 m, a zenith angle of 50° and no glass in the LDC. Fortunately, since the refractive index of air changes slowly in this band, no dispersion correction is required for the IR. Similar calculations can show that this is also the case for the angular change introduced by atmospheric refraction. Unfortunately, since both an ARC and an LDC are required for the visible band, the effect of which is to move the fringes

DIFFERENTIAL PATH CONSIDERATIONS

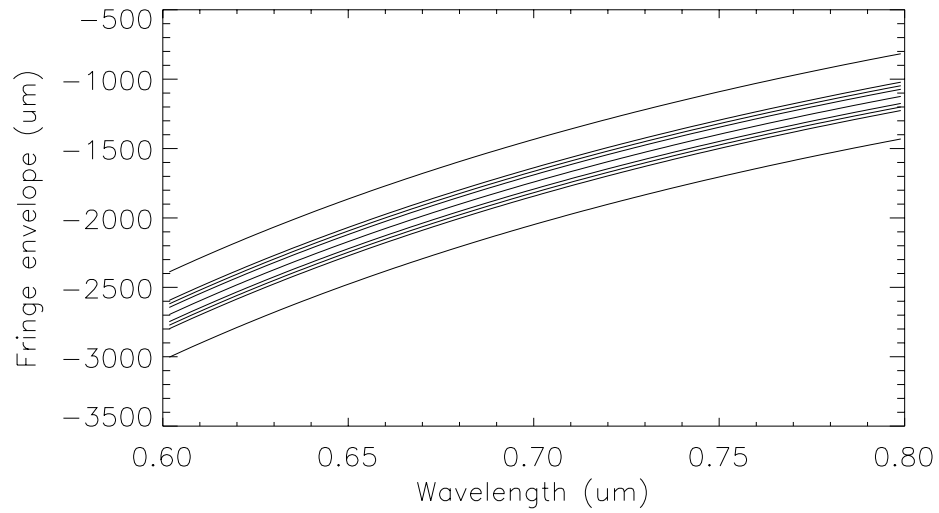


FIGURE N.4. The fringe envelope for a baseline of 350 m and a zenith angle of 50° without dispersion correction. The central line represents the center of the envelope, the next pair of lines the 95% point, the next pair the 90% point, the next pair the 85% point, and the outermost lines the first zero.

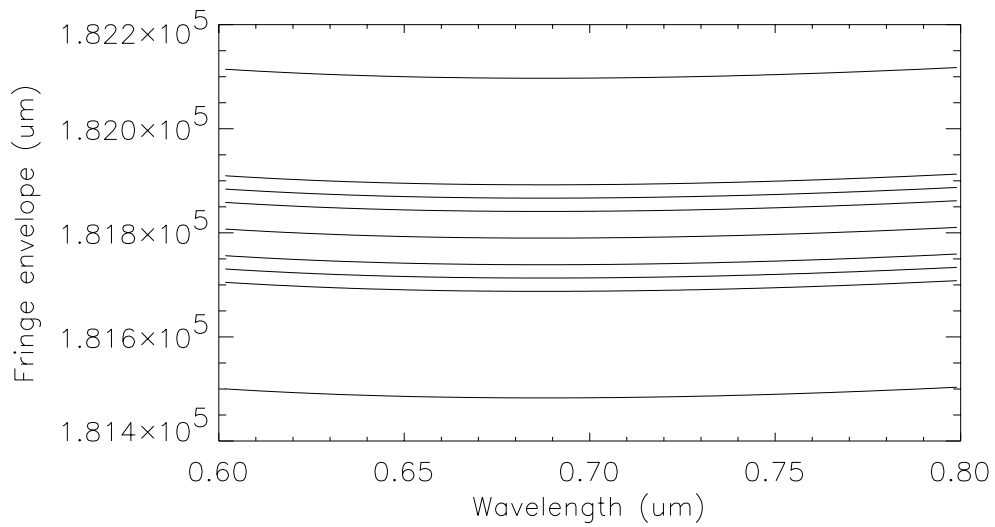


FIGURE N.5. The fringe envelope for a baseline of 350 m and a zenith angle of 50° with dispersion correction. The central line represents the center of the envelope, the next pair of lines the 95% point, the next pair the 90% point, the next pair the 85% point, and the outermost lines the first zero.

THE CHARA ARRAY

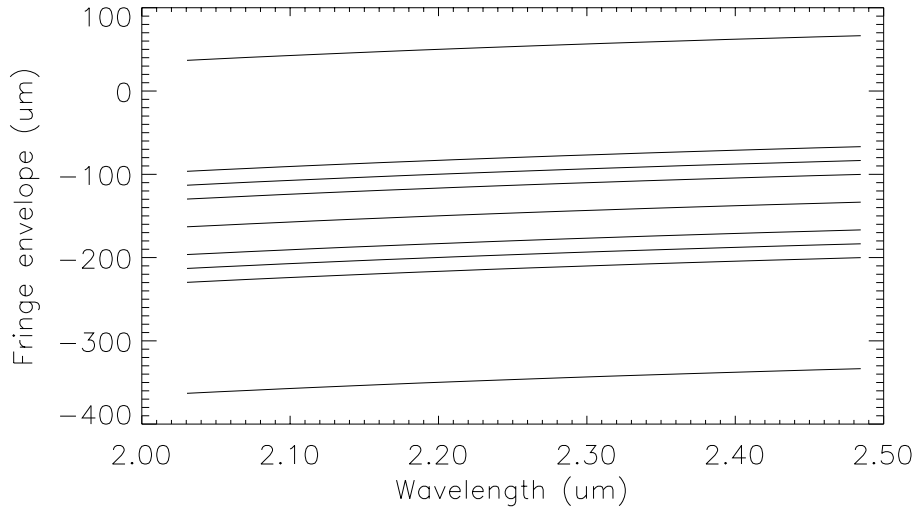


FIGURE N.6. The IR fringe envelope for a baseline of 350 m and a zenith angle of 50° degrees without dispersion correction.

several centimeters, it is unlikely that it will be possible to simultaneously observe in both bands.

It has been suggested by S. Ridgway that it would be advantageous, for example when imaging YSOs, to use the visible system for fringe tracking while using the IR system for visibility measurements. Since the LDC will move the visible light fringes several centimeters away from the IR fringes, this may be difficult. However, if one is willing to forgo using the visible system for visibility measurements and use it only for fringe tracking, this problem can be solved by simply removing the LDC altogether. For example, in Figure N.7 the IR fringes are plotted for a baseline of 100 meters and a zenith angle of 30° in solid lines. Superimposed on these lines are dashed and dotted lines representing the position of the visible fringes in the band 0.9 – 1.0 microns without dispersion correction. The IR fringes lie almost completely within the 10% loss area of the visible fringes. It should therefore be possible to offset track using the 0.9 – 1.0 micron band while doing imaging in the IR band. This scheme will also work at other visible bands although with increased visibility losses.

N.5. FIELD OF VIEW

From Equation N.18 we see that the contribution to fringe displacement due to changing the field of view angle α is

$$l_{\text{FOV}} = \frac{\Delta\nu\alpha B \cos\theta}{\nu_0\Delta n_{\text{air}} + n_{\text{air}}(\nu_0)\Delta\nu}. \quad (\text{N.21})$$

If we say that we are allowed to go to some fraction of the envelope F , then we can write

$$l_{\text{FOV}} = F\Delta l \quad (\text{N.22})$$

which, after solving for α gives

$$\alpha = \frac{2F}{\Delta\nu B \cos\theta} \quad (\text{N.23})$$

DIFFERENTIAL PATH CONSIDERATIONS

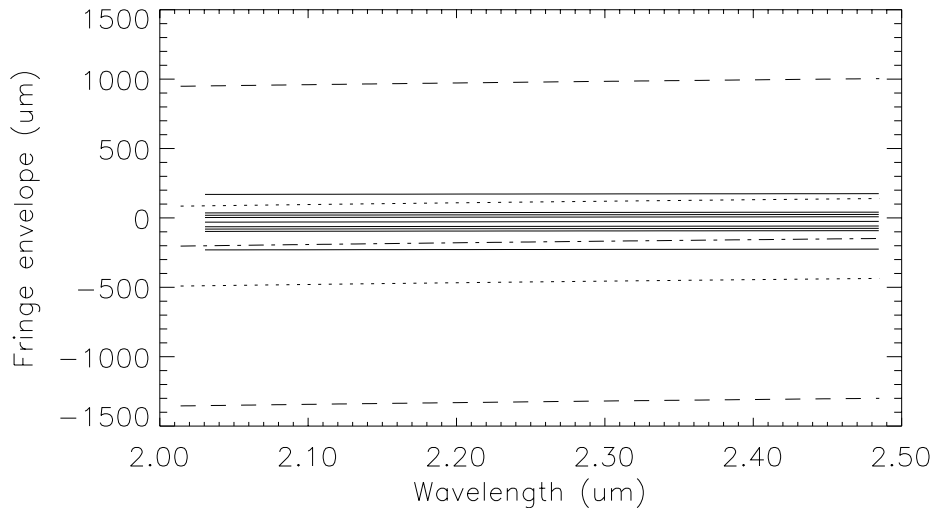


FIGURE N.7. The IR fringe envelope (solid lines) for a baseline of 100 m and a zenith angle of 30° without dispersion correction. The fringes for a visible band of $0.9\text{-}1.0\mu\text{m}$ for the same situation and no dispersion correction are superimposed with dotted and dashed lines. Note that even without dispersion correction, the IR fringes lie completely within the range of the visible fringes.

from which we can calculate the usable field of view for the array. We must also remember that if the two Airy patterns created by the beams do not overlap, no fringes will be seen at all. This gives us an absolute maximum field of view of $\frac{2.4\lambda}{D}$ where in our case the diameter $D = 1\text{ m}$. Since we are planning to use a CCD detector with on-chip binning to produce pixels evenly spaced in the band, the field of view in a given band will be constant across wavenumber and only a function of the projected baseline. Two examples are given in Figure N.8, one for the 20 pixel IR band of 2.0 to 2.5 microns and the other for the 128 pixel visible band of 0.6 to 0.8 microns. The fraction of visibility for the IR band was 50% while that of the visible was 5%.

N.6. CONCLUSION

This analysis has shown that dispersion can be corrected to a large extent by a single piece of BK7 glass. This technique should be expandable to the full seven telescopes planned for the CHARA Array. Atmospheric refraction was shown to be a second-order effect for the current aperture size of 1 m and can be corrected using Risley prisms at the back end of the interferometer. This may not be true if we choose to go to larger apertures. In the IR band neither an ARC nor an LDC will be required, although due to the fringe displacement in the visible band caused by dispersion correction, it will probably not be possible to observe in the visible and IR bands simultaneously. It will, however, be possible to use the $0.9\text{-}1.0\mu\text{m}$ band with dispersion correction for fringe tracking while doing science in the IR band. The field of view of the instrument is restricted by the size of the Airy pattern on baselines of less than approximately 100 m and becomes smaller for larger baselines due to the optical path length difference introduced by the angular offset. Nevertheless, based on these figures, it should be possible to image YSOs.

THE CHARA ARRAY

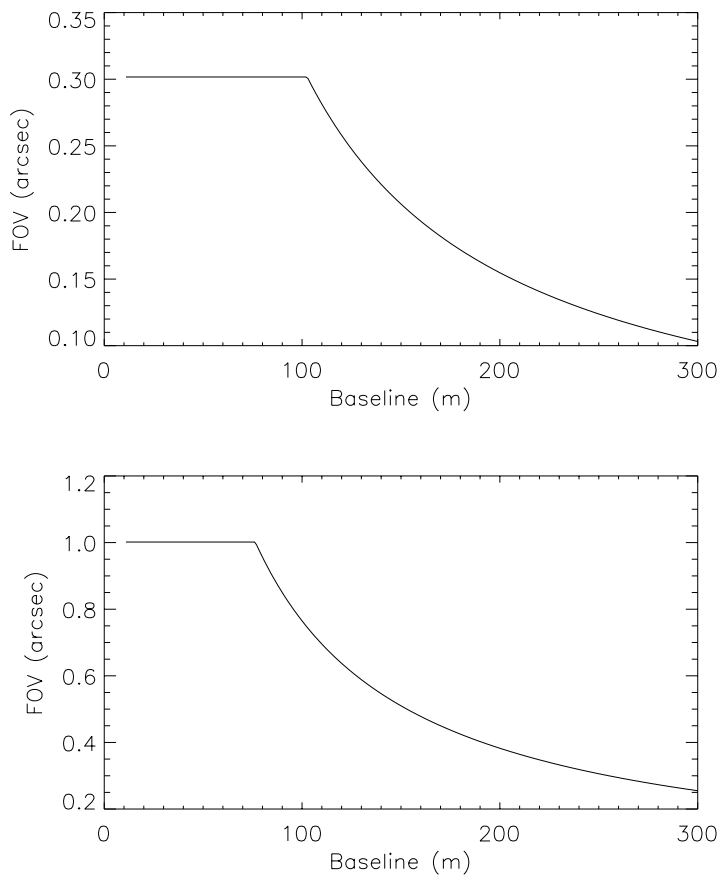


FIGURE N.8. The field of view for the visible (top) and IR (bottom) bands. For the smaller baselines the FOV is restricted by the Airy disk size while for the large baselines differential optical paths start to dominate.

N.7. REFERENCES

- Ling, L., 1990, "Air Path Mismatch Compensation", *N.R.O. Tech Report*, OIPTR 90-001
Tango, W.J., 1990, "Dispersion in Stellar Interferometry", *Appl. Optics*, **29**, 516
Traub, W., 1990, "Visibility Loss with an Air Filled Delay Line", IOTA Internal Report